Climate Dynamics (2003) 20: 175–191
DOI 10.1007/s00382-002-0268-2

F. Molteni

Atmospheric simulations using a GCM with simplified physical parametrizations. I: model climatology and variability in multi-decadal experiments

Received: 7 March 2002 / Accepted: 4 June 2002 / Published online: 5 September 2002

Abstract This work describes the formulation and climatology of an atmospheric general circulation model (GCM) of intermediate complexity, based on a spectral primitive-equation dynamical core and a set of simplified physical parametrization schemes. The parametrization package has been specially designed to work in models with just a few vertical levels, and is based on the same physical principles adopted in the schemes of state-of-the art GCMs. The parametrized processes include large-scale condensation, convection, clouds, short-wave and long-wave radiation, surface fluxes and vertical diffusion. In the current configuration, the model (nicknamed SPEEDY, from Simplified Parametrizations, primitivE-Equation DYnamics") has five vertical levels and a spectral truncation at total wave number 30 (T30L5). The top vertical level (crudely) represents the stratosphere, the bottom one the planetary boundary layer. Computationally, SPEEDY requires (at least) one order of magnitude less CPU time than a state-of-the-art GCM at the same horizontal resolution, and is therefore suitable for studies of inter-decadal or inter-centennial variability. Statistics of the model mean state and variability are computed from an ensemble of 41-year simulations forced by observed sea-surface temperatures in the period 1952–1992. The model mean state is closer to the observed climatology during the (boreal) winter than during summer. In winter (i.e. December to February, DJF), the model underestimates the amplitude of the Northern Hemisphere stationary wave pattern, particularly in the European-Atlantic sector. Some aspects of the systematic error of SPEEDY are in fact typical of many GCMs, although the error amplitude is stronger than in state-of-the-art models. On the other hand, the global distribution of precipitation in DJF is quite realistic, and compares well with that of more complex GCMs. In summer (June to August), a strong negative bias in the mid-tropospheric temperature generates a Northern Hemisphere circulation with some springtime characteristics. In particular, the position of the Tropical Convergence Zone in the Indian Ocean remains too far south, leading to a deficient simulation of the monsoon circulation over South Asia. The simulated variability during the northern winter is reasonably realistic as far as the spatial distribution is concerned, although some underestimation in the intensity can be found, particularly in the low-frequency range and in the Atlantic sector. The atmospheric response to ENSO events is also weaker than observed, although the spatial patterns of the rainfall and geopotential response in the Pacific sector are in phase with their observed counterparts. In the Atlantic/Eurasian region, the spatial patterns associated with the interdecadal trends in the simulated and observed large-scale circulation show a clear positive correlation, consistent with the hypothesis of a positive ocean–atmosphere feedback on decadal time scales.

1 Introduction

General circulation models (GCMs) are essential tools for current research on dynamical climatology. The amazing increase in the availability of computing resources, which has occurred in the last few decades, allows numerical simulations of the Earth's climate on decadal and centennial time scales with models of high complexity and resolution. These simulations are particularly important for the understanding of the interactions between the atmosphere, the ocean and other components of the climate system (e.g. Randall 2000), and for investigations of possible future climate scenarios based on different hypotheses for anthropogenic emissions of greenhouse gases (e.g. IPCC 2001).

The complexity and sophistication of state-of-the-art GCMs allow a fairly realistic description of many

F. Molteni
Abdus Salam International Centre for Theoretical Physics,
Strada Costiera 11, 34014 Trieste, Italy
E-mail: moltenif@ictp.trieste.it

features of the atmospheric circulation. The price to be paid for such a sophistication is that diagnosing the dynamical and physical origin of atmospheric phenomena from GCM simulations may be almost as difficult as using the real atmospheric data. Also, from the point of view of software architecture, today's most advanced GCMs are very complex pieces of code. Indeed, for scientists not directly involved in model development, it is sometimes difficult to get a proper understanding of a GCM's code structure in order to perform specific sensitivity experiments.

For these and other reasons (ranging from intellectual challenge to computational constraints), climate models of low and intermediate complexity are still needed in order to simulate climatic phenomena in a simplified and easily controlled environment. Of course, this is not a new situation. Simplified models have always played an important role in physical and dynamical climatology. However, while in the past simplified models have been mostly applied to idealized spatial domains (for example, in the case of models of the zonally symmetric atmospheric circulation), recently a number of research groups have developed models with a simplified formulation but enough spatial resolution to represent the global circulation in a realistic geographical setting (e.g. Opsteegh et al. 1998; Forster et al. 2000).

The purpose of this work is to describe the formulation and climatology of an atmospheric GCM of intermediate complexity, based on a spectral primitive-equation dynamical core (Held and Suarez 1994) and a set of simplified physical parametrization schemes. The parametrization schemes have been specially designed to work in models with just a few vertical levels, starting from the same fundamental physical principles which are at the base of the more sophisticated schemes of state-of-the-art GCMs. In particular, the schemes do not assume any empirical heating profile, and therefore are suitable to represent the variations of the atmospheric energy sources/sinks as a function of modelled energy fluxes at the lower and upper boundaries, and of the internal distribution of temperature and moisture.

The model (known as SPEEDY, for "Simplified Parametrizations, primitivE-Equation DYnamics") is currently being used in a configuration with five vertical levels and a triangular truncation of horizontal spectral fields at total wave number 30 (T30L5). Of the five vertical layers, the top one (crudely) represents the stratosphere, the bottom one the planetary boundary layer (PBL), with three layers in the "free" troposphere. It is felt that this is the minimal vertical resolution that allows the development of reasonably realistic parametrization schemes. The model is designed to require (at least) one order of magnitude less CPU time than a state-of-the-art GCM at the same horizontal resolution, and is therefore suitable for studies of inter-decadal or inter-centennial variability (coupling with ocean models of different complexity is planned for the near future).

The study is structured as follows. Section 2 gives an overview of the structure of SPEEDY, including a brief description of the dynamical core, the basic principles of the physical parametrizations, and the specification of boundary conditions. Section 3 compares the model climatology, obtained from an ensemble of 40-year simulations with prescribed sea-surface temperature (SST), with its observed counterpart. Section 4 provides a basic statistical analysis of the modelled variability on intraseasonal, interannual and interdecadal time-scales. The results are discussed in Sect. 5, which includes an outline of future development work aimed at improving the model performance. A detailed description of the parametrization schemes is given in an Appendix, available from the web site "http://www.ictp.trieste.it/~moltenif/speedy-doc.html".

2. Model formulation

2.1 The dynamical core

The SPEEDY model is based on a spectral dynamical core developed at the Geophysical Fluid Dynamics Laboratory (see Held and Suarez 1994). It is a hydrostatic, σ-coordinate, spectral-transform model in the vorticity-divergence form described by Bourke (1974), with semi-implicit treatment of gravity waves. The basic prognostic variables are vorticity (*Vor*), divergence (*Div*), absolute temperature (T) and the logarithm of surface pressure ($\log(p_s)$); the code also computes the evolution of a number of additional variables which are simply advected by the dynamical core (with sources and sinks specified by the physical parametrizations). In SPEEDY, the only additional variable currently used is specific humidity (Q).

The time stepping uses a leapfrog scheme, with a time filter (Robert 1966) to suppress the computational mode. Horizontal hyper-diffusion of *Vor*, *Div*, T and Q has the form of the third-power of the Laplacian, applied on σ surfaces; a corrective term which simulates diffusion on pressure surfaces is used for T and Q, to avoid spurious diffusion over topography.

The horizontal resolution used for the experimentation described here corresponds to a triangular spectral truncation at total wave number 30 (T30), with a standard gaussian grid of 96 by 48 points. In the current formulation of SPEEDY, five vertical layers are used, with boundaries (half-levels) at σ values of 0, 0.15, 0.35, 0.65, 0.90 and 1.

The prognostic variables (apart from $\log(p_s)$) are specified at σ levels intermediate between the upper and lower boundaries (known as full levels), namely at σ 0.075, 0.25, 0.50, 0.775 and 0.95. In practice, the top and the bottom layer provide a "bulk" representation of the stratosphere and the planetary boundary layer (PBL) respectively. The output data are post-processed on pressure levels at 70, 250, 500, 775 and 925 hPa.

2.2 Overview of physical parametrizations

A set of physical parametrization schemes has been developed starting from basic principles used in more complex GCMs, with a number of simplifying assumptions which are suited to a model with a coarse vertical resolution. A brief description of processes represented by the schemes is given here; a more detailed and quantitative description can be found in Appendix A, on the web site http://www.ictp.trieste.it/~moltenif/speedy-doc.html.

2.2.1 Convection

A simplified mass-flux scheme is activated where conditional instability is present (namely, where saturation moist static energy decreases with height between the lowest layer, PBL, and the upper-tropospheric layers), and where humidity in the PBL exceeds

a prescribed threshold. The cloud-base mass flux (at the top of the PBL) is such that the PBL humidity is relaxed towards the threshold value on a time-scale of 6 h. Detrainment occurs only at the cloud-top level (determined by the conditional instability criterion), while entrainment occurs in the lower half of the troposphere. The air in the updrafts is assumed to be saturated.

2.2.2 Large-scale condensation

When relative humidity exceeds a σ-dependent threshold, specific humidity is relaxed towards the corresponding threshold value on a time scale of 4 h, and the latent heat content removed from the atmosphere is converted into dry static energy.

2.2.3 Clouds

Cloud cover and thickness are defined diagnostically from the values of relative and absolute humidity in an air column including all tropospheric layers except the PBL.

2.2.4 Short-wave radiation

The shortwave radiation schemes uses two spectral bands, one of which represents the near-infrared portion of the spectrum. Radiation is reflected at cloud top and at the surface; the cloud albedo is proportional to the total cloud cover. The shortwave transmissivities of the model layers are functions of layer mass, specific humidity and cloud cover.

2.2.5 Long wave radiation

The longwave radiation schemes uses four spectral bands, one for the atmospheric "window" and the other ones for the spectral regions of absorption by water vapour and carbon dioxide. For each layer, transmissivities in the four bands are defined as a function of layer mass and humidity. The effect of clouds is represented as a descrease in the transmissivity of the "window" band, as a function of cloud cover. The downward emission from each layer is computed as a weighted function of the temperature at the full level and of the (interpolated) temperature at the half-level below. For the upward emission, the temperature at the full level and at the half-level above is used.

2.2.6 Surface fluxes of momentum and energy

Surface fluxes are defined by bulk aerodynamic formulas with different exchange coefficients between land and sea. Coefficients for (sensible and latent) heat fluxes also depend on a simple stability index, while the coefficient for the momentum flux over land is a function of topographic height.

2.2.7 Vertical diffusion

This is composed of three terms: a redistribution of dry static energy and moisture between the two lowest model layers, which simulates shallow convection in regions of conditional instability; a diffusion of water vapour in stable conditions which acts in the lower troposphere, depending on the vertical profile of relative humidity; and a diffusion of dry static energy in case the lapse rate approaches (or exceeds) the dry-adiabatic limit.

2.3 Boundary conditions

As any atmospheric model, SPEEDY requires appropriate boundary conditions to determine the fluxes of momentum, heat and moisture at the surface, and the flux of incoming solar radiation at the top of the atmosphere.

At the surface, in addition to topographic height and (fractional) land–sea mask, the model requires climatological fields of the following variables:

1. Sea surface temperature (SST)
2. Sea ice fraction
3. Surface temperature in the top soil layer (about 10 cm)
4. Moisture in the top soil layer and the root-zone layer
5. Snow depth
6. Bare-surface albedo (in the absence of snow or sea ice)
7. Fraction of land-surface covered by vegetation

For the last two fields, annual-mean values are used, while all other fields are specified as monthly means and are linearly interpolated to get daily-updated values.

The bare-surface albedo is linearly combined with assigned values of sea-ice and snow albedo to get a net surface albedo, using weights which are linearly dependent on sea-ice fraction and snow cover respectively. Similarly, the soil moisture in the top soil layer and in the root zone are linearly combined (using the vegetation fraction) to define a soil moisture availability index, which is used to compute evaporation over land. (See Appendix A.6 for more detail.)

All climatological fields have been computed by averaging the corresponding data from the European Centre for Medium-Range Weather Forecasts' re-analysis (ERA; see Gibson et al. 1997) in the period 1981–90. This period has been chosen (instead of the full 1979–93 period cover by ERA) to have a better balance between warm and cold ENSO events in the SST field.

In the model version described, no anomalies are allowed in the land-surface parameters, although a scheme to define land-surface temperature from a simple energy balance model is being tested for future versions. On the other hand, the model allows a time-varying SST anomaly to be superimposed to the climatological SST; the anomaly can be either specified from an input file or computed by a coupled ocean model. In Sect. 3, the model climatology obtained with prescribed SST anomalies will be described, while results obtained with a coupled model of the oceanic mixed-layer will be reported elsewhere.

At the top-of-the-atmosphere, the incoming flux of solar radiation is computed daily from astronomical formulae (the model has no daily cycle). Empirical, seasonally varying functions are used to define the absorption of solar radiation by ozone in the stratosphere, and the latitudinal variations of the optical depth for solar radiation depending on the daily averaged zenith angle. The use of a proper ozone climatology is planned for future model versions.

3 Model climatology

3.1 Definition of climatological statistics

The model climatology decribed below has been deduced from an ensemble of three multi-decadal integrations covering the period from 1952 to 1992 (included). The climatology used for all surface fields has been described in the previous section. SST anomalies for the 1952–92 periods have been computed from the EOF-reconstructed SST dataset by Smith et al. (1996), and have been superimposed to the SST climatology. The different ensemble members have been started from model-generated initial conditions corresponding to different times of a simulation with climatological SST. Initial times are separated by 6 months, and all runs cover a common 41-year period from January 1952 to December 1992.

It should be pointed out that the procedure used to generate the SST fields in the model integrations produces some inconsistencies with the actual SST fields (of the order of a few tenths of degree), since the multi-decadal SST climatology of Smith et al. (1996) differs from the 10-year ERA climatology. On the other hand, using different climatologies for different surface parameters would also lead to inconsistencies. To be coherent with our choice of surface boundary conditions, the model mean state will be validated against ERA (or other data sources for the ERA period), while estimates of modelled interannual variability will be validated against the National Centers for Environmental Prediction/National Center for Atmospheric Research (NCEP/

NCAR) reanalysis in the 1952–92 period (see Kalnay et al. 1996; Kistler et al. 2001).

In order to reduce the data storage requirements, the model output has been mainly archived as monthly-mean statistics (mean and variances/covariances), with 5-day mean statistics saved only for the ERA period. Therefore, indices of intraseasonal variability refer to the same period used for the validation of the mean state.

3.2 Mean state in the boreal winter

In this subsection, the model performance in representing the time-mean state of the atmosphere during the boreal winter (December–January–February, DJF herafter) will be assessed. Figure 1 compares cross sections of zonal-mean temperature from the SPEEDY integrations (Fig. 1a) and from ERA (Fig. 1b). In order to highlight the meridional temperature gradient, a reference temperature has been defined at each pressure level as the global mean temperature from the ERA dataset, and has been subtracted from both model and analysis data. It should also be noted that the ERA cross section has been computed using only data at the five pressure levels represented by the model. In this way, a proper comparison with model results can be achieved, although differences may arise with respect to similar cross-sections obtained using all ERA vertical levels.

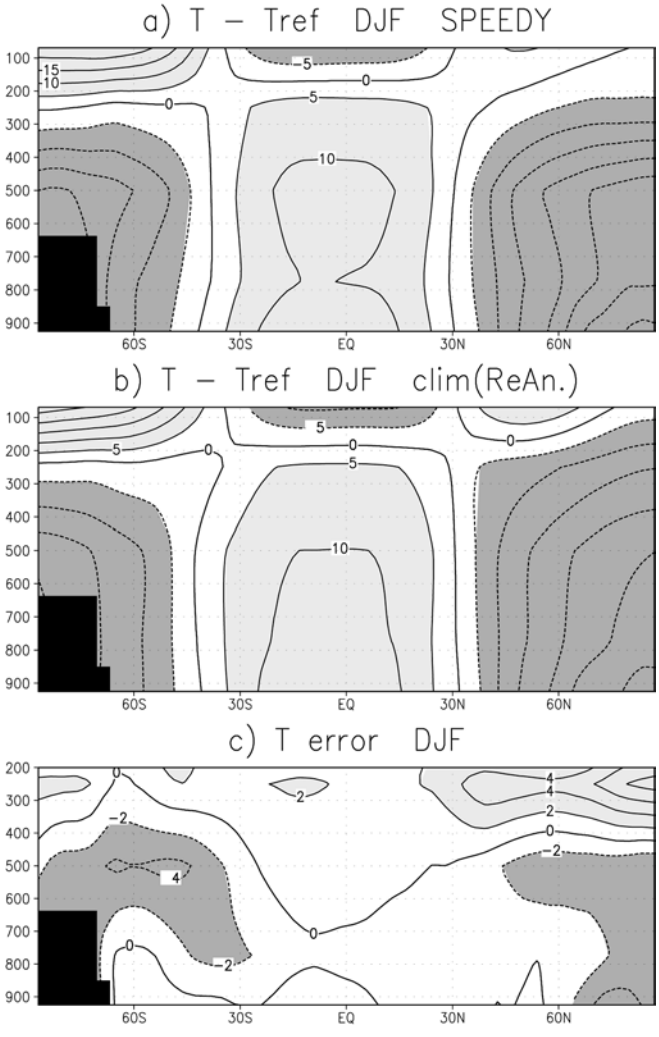

Fig. 1 Cross section of zonal-mean temperature in DJF, from **a** SPEEDY ensemble, and **b** ECMWF reanalysis (ERA). At each pressure level, a reference temperature defined as the ERA global-mean value is subtracted from both model and ERA data. **c** Mean model error (SPEEDY – ERA) in the tropospheric levels. Contour interval: 5 K in **a**, **b**, 2 K in **c**, with negative contours *dashed*. In *each panel*, values greater than one positive contour interval, and less than one negative contour interval are *shaded*

The comparison between SPEEDY and ERA data shows that the model reproduces the tropospheric thermal structure to a good degree of accuracy, although the decrease of the meridional temperature gradient with height is not monotonic as in the analysis (it is actually slightly stronger at 500 hPa than at 775 hPa. The reversal of the temperature gradient in the stratosphere is also reasonably simulated, although the presence of just one stratospheric layer (affected by empirical forcing and dissipation terms) implies that strict quantitative comparisons with analysis are not meaningful in such a layer. For this reason, the model systematic error (defined as the difference between the modelled and analyzed mean states) is plotted in Fig. 1c only for the troposphere. A cold bias (with a maximum amplitude of –4 K at 60°S) is present in the midlatitude and polar regions of both hemispheres at 500 hPa, which causes the stronger-than-observed meridional temperature gradient at this level. On the other hand, an upper-tropospheric warm bias is evident in the extratropics of the Northern Hemisphere only (experiments suggest that this is due to insufficient radiative cooling in nearly dry regions of the atmosphere). Overall, the tropospheric temperature bias of the model is acceptable, when compared to similar statistics from much more compex GCMs (see e.g. Fig. 4 in Brankovic and Molteni 1997).

Cross sections of zonal-mean zonal wind for SPEEDY and ERA are displayed in Fig. 2. Again, one should not expect the model to provide an accurate description of stratospheric wind with such a coarse vertical resolution. On the other hand, the simulation of tropospheric zonal wind is quite realistic, with a nearly correct amplitude and location of the upper-tropospheric jet maxima in both hemispheres, and a good simulation of the vertical tilt of the region of maximum zonal wind. The location of the lower-tropospheric easterly maximum is also well represented. The tropospheric model bias, shown in Fig. 2c, has a maximum of about 4 m/s in the northern midlatitudes; in the Southern Hemisphere, a northward shift of the jet structure is associated with a negative bias exceeding –8 m/s at all tropospheric levels around 50°S, and an upper-tropospheric bias of 6 m/s around 30°S.

Since the coupling of SPEEDY to a model of the upper-ocean circulation is forseen in the near future, the ability of the model to simulate the distribution of near-surface winds should be carefully assessed. Figure 3 shows global maps of 925-hPa zonal winds from SPEEDY and ERA climatologies, and their difference (this pressure level is very close to the lowest model level at $\sigma = 0.95$). Qualitatively, the location of the main regions of westerly and easterly flow are reasonably well represented, including the region of westerlies in the tropical Indian Ocean. Looking in more detail at the difference map (Fig. 3c), a widespread positive bias in the westerlies around 40°N is evident, with a maximum amplitude exceeding 6 m/s over southern Europe. In fact, over the North Atlantic, the region of strong westerlies (exceeding 6 m/s) associated with the storm track has a more zonal orientation in the model simulation than in the analysis, and extends too far east into the Mediterranean region. This error is typically found in many GCMs, although with a different (and usually smaller) amplitude. In the tropics, the strength of the easterly flow is underestimated in the east Pacific, and the westerlies over Indonesia are also weaker than observed. In the southern extratropics, the northward shift of the jet position, noted in the cross sections of Fig. 2, is reflected in a considerable negative bias around 50°S.

If the systematic error of SPEEDY is larger than state-of-the-art GCMs as far as near surface winds are concerned, the simulated distribution of precipitation during the boreal winter compares more favourably with those of more sophisticated models. In Fig. 4, the global rainfall simulated by SPEEDY is assessed against the climatology of the CMAP (Climate Prediction Center Merged Analysis of Precipitation) dataset prepared by

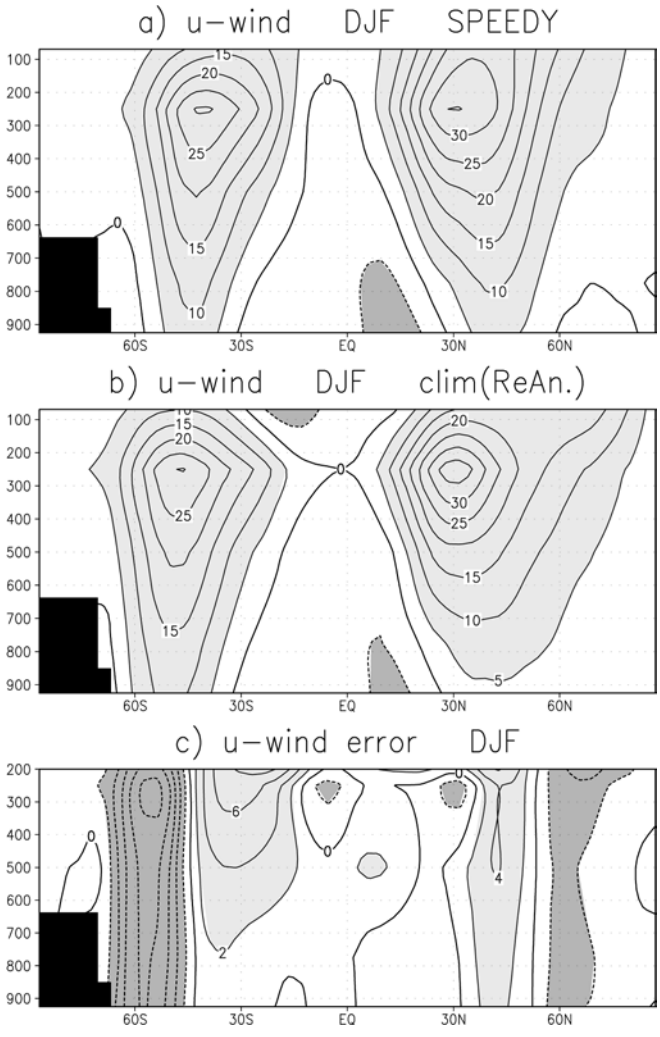

Fig. 2 Cross section of zonal-mean wind in DJF, from **a** SPEEDY ensemble, and **b** ERA. **c** Mean model error (SPEEDY – ERA) in the tropospheric levels. Contour interval: 5 m/s in **a**, **b**, 2 m/s in **c** negative contours *dashed*, *shading* as in Fig. 1

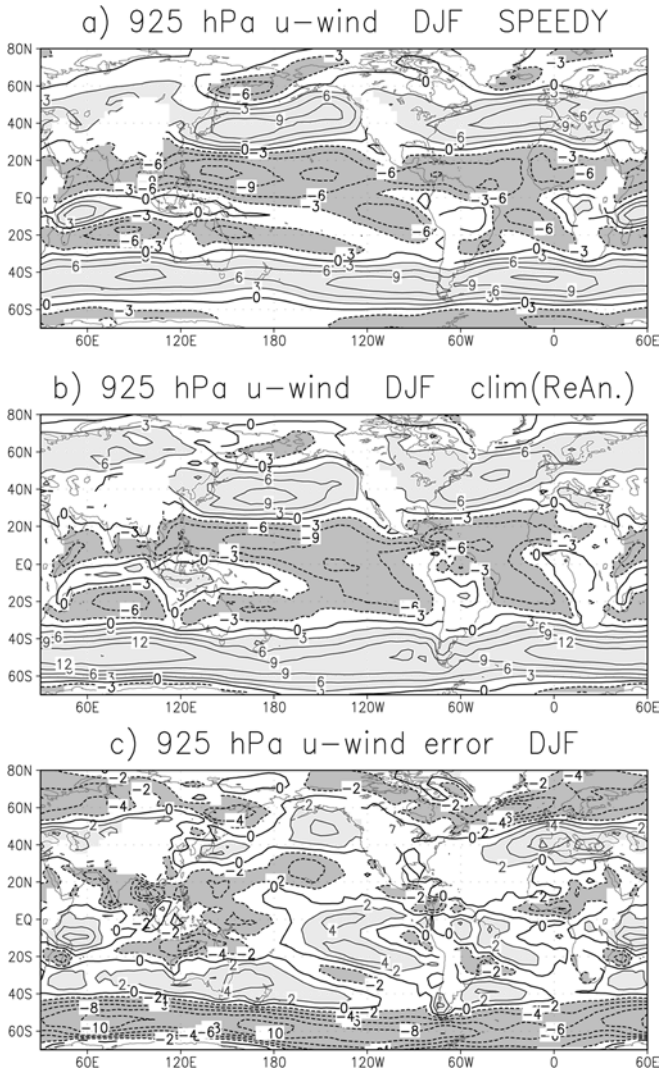

Fig. 3 Mean zonal wind at 925 hPa in DJF, from **a** SPEEDY ensemble, and **b** ERA. **c** Mean model error (SPEEDY – ERA). Contour interval: 3 m/s in **a**, **b**, 2 m/s in **c** negative contours *dashed*, *shading* as in Fig. 1. Regions of high topography (where data are extrapolated below the surface) are *blanked out*

Xie and Arkin (1997). In the lowest panel, the zonal-mean rainfall is also compared with the ERA-15 climatology (for consistency, CMAP data have been averaged over the ERA period in Fig. 4c). The model reproduces all major features of the global rainfall distribution, including the dry areas on the eastern side of the subtropical oceans. In the tropics, the relative strength of the precipitation areas over the Indian and west Pacific oceans is reversed, with an underestimation of the intensity of the South Pacific Convergence Zone (SPCZ). Also, a stronger-than-observed rainfall maximum is simulated over the Congo Basin, while over South America rainfall has a rather 'spotty' distribution. Still, in view of the rather basic formulation of SPEEDY's convection and large-scale condensation schemes, the agreement with observations is remarkable. When the zonal mean rainfall is considered, in many regions the difference between the SPEEDY and CMAP distributions is comparable to the difference between the CMAP and ERA climatologies.

In atmospheric models of intermediate complexity, schemes with widely different levels of sophistication have been used for the parametrization of radiative processes. Since the radiation scheme of SPEEDY is based on a simplified radiative transfer model, the simulated field of outgoing longwave radiation (OLR) provides useful indications on the performance of such a scheme. In Fig. 5, the simulated OLR is validated against observational data from NOAA satellites, made available by NCEP as monthly mean fields. Although the large-scale distribution shows clear differences between dry and convective regions in the tropics, the quantitative agreement with observations is not as good as for the precipitation field. In the tropics, OLR values over the continental convective regions are not as low as in observations, while they are lower than observed over the east Pacific. The main discrepancy, however, is represented by the too large OLR values over the extratropical oceans, which clearly show up in the zonal-mean profile shown in Fig. 5c. Since the regions where the OLR bias is stronger are also characterized by a negative temperature bias in the mid-troposphere, it may be argued that such a cold bias is originated by some deficiency of the long-wave radiation scheme, or by errors in the vertical distributions of clouds and water vapour in the extratropical storm-track regions, which affect the optical thickness of the atmospheric layers.

Focusing now on the Northern Hemisphere circulation, Fig. 6 compares the model climatology of 500-hpa geopotential height with the ERA climatology. Full fields (and the corresponding mean error) are shown in the left column, while panels on the right column show the eddy component of the fields (i.e their

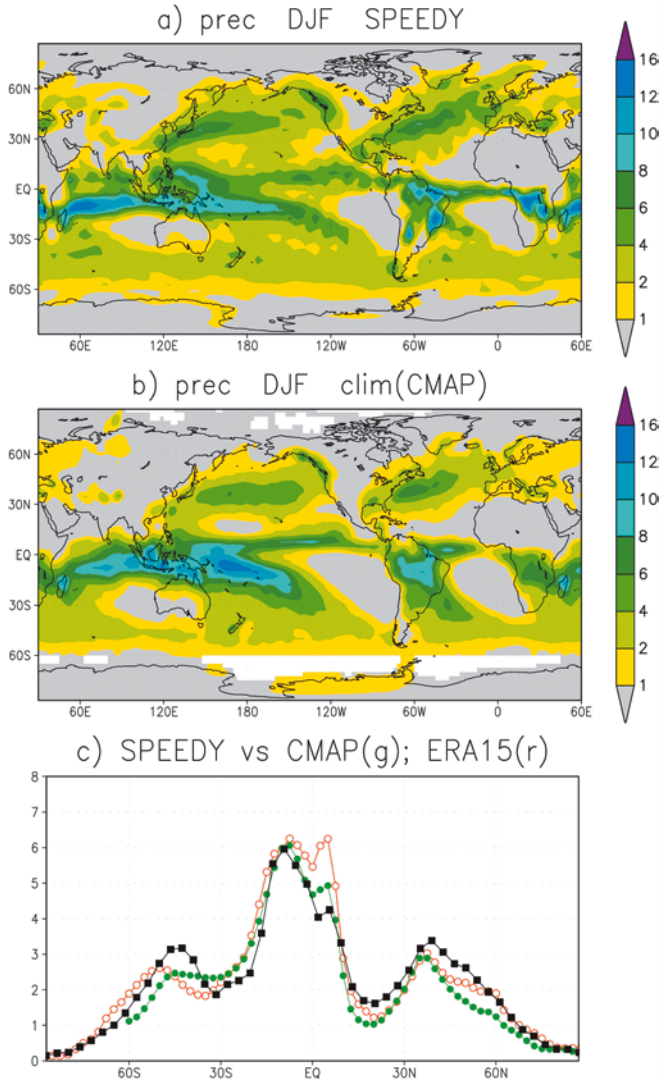

Fig. 4 Mean precipitation in DJF (in mm/day), from **a** SPEEDY ensemble, and **b** CMAP data averaged over the ERA period. **c** Zonal-mean distribution from SPEEDY (*black*), CMAP (*green*) and ERA (*red*)

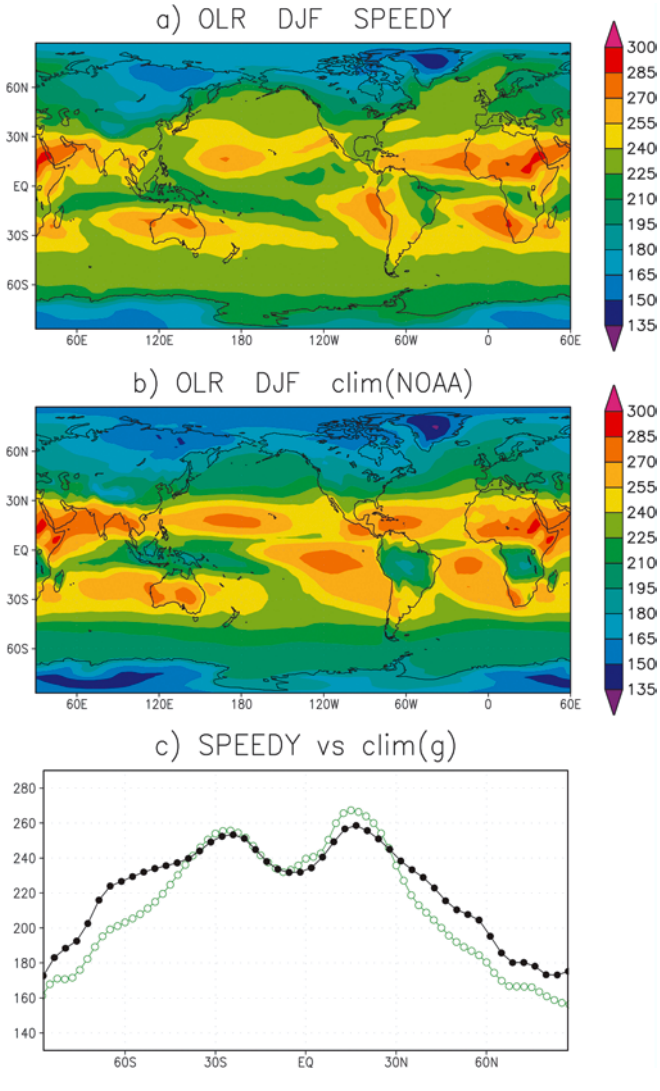

Fig. 5 Mean outgoing longwave radiation (OLR) in DJF (in W/m^2), from **a** SPEEDY ensemble, and **b** NOAA satellite observations averaged over the ERA period. **c** Zonal-mean distribution from SPEEDY (*black*) and NOAA data (*green*)

deviations from zonal means). Just looking at the full height fields in Fig. 6a, b, it is evident that the model underestimates the amplitude of the stationary eddies. Comparing the eddy fields in Fig. 6d, e, one finds that the simulated amplitude is about 30% less than the observed value in the Pacific sector, about half of the observed amplitude over the eastern part of North America and in the European-Atlantic region (where the eddy maxima are also shifted southwards). In fact, the systematic model error is dominated by its eddy component (see Fig. 6c, f), which is negatively correlated with the observed stationary wave pattern. It should be mentioned that, while the amplitude of the stationary wave pattern in the Pacific proved to be rather sensitive to changes in the physical parametrization schemes, the underestimation of the Atlantic wave pattern has remained almost unchanged in a large number of such sensitivity experiments. Longitude-height cross sections of observed and simulated temperatures around 50°N (not shown) indicate that the zonal temperature asymmetries associated to the land–sea distribution decrease too strongly with height in the model over the Atlantic sector. However, whether this is due to a still uncorrected deficiency of the parametrization schemes, or has a more fundamental dynamical origin, is the subject of current investigation.

3.3 Mean state in the boreal summer

The difficulty of achieving an accurate simulation of the atmospheric circulation during the boreal summer is a fairly common experience among numerical modellers. The simulation of thermally driven circulation systems, such as the monsoons, represents a harsh test even for very sophisticated parametrization packages. Indeed, recent surveys of GCM performances in simulating tropical circulations (e.g. Sperber and Palmer 1996) have revealed substantial systematic errors in many state-of-the-art models.

In such a situation, it is not suprising to find that SPEEDY's simulation of the circulation during the boreal summer (June–July–August, JJA hereafter) is much less satisfactory than its wintertime counterpart. Notably, the absence of a diurnal cycle in the model makes it difficult to achieve an accurate representation of convection and sub-grid-scale vertical heat transport over the continents.

These difficulties are clearly reflected in the cross section of zonal mean temperature, shown in Fig. 7. As for the winter data in Fig. 1, the ERA global mean at each pressure level has been subtracted to simulated and analyzed data. As in DJF, the model overestimates the strength of the meridional temperature gradient in the extratropical regions at 500 hPa. In the Northern

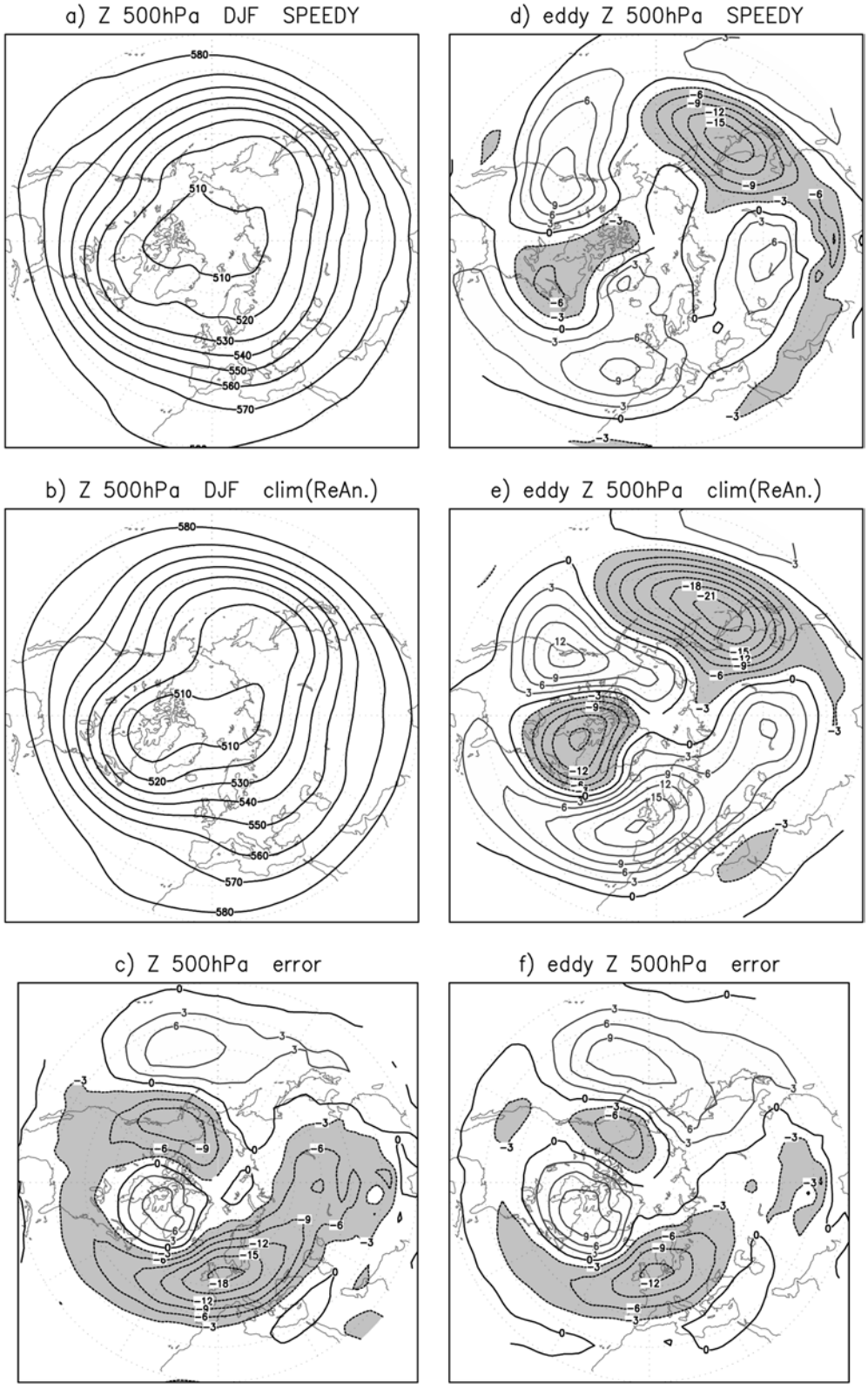

Fig. 6 Mean geopotential height at 500 hPa in DJF, from **a** SPEEDY ensemble, and **b** ERA. **c** mean model error (SPEEDY – ERA). Contour interval: 10 dam in **a**, **b**, 3 dam in **c**. **d**, **e**, **f** show the eddy component of the fields in **a**, **b**, **c** respectively, with contour interval 3 dam. Negative contours *dashed*, *shading* as in Fig. 1

Hemisphere, this error is much greater than in winter, leading to a widespread cold bias which exceeds –8 K in the polar mid-troposphere. Large temperature biases (negative in the lower troposphere, positive above 500 hPa) are also found over Antarctica. It may also be noticed that the model simulation of lower-stratospheric temperature shows a much stronger symmetry between the two hemispheres than is actually observed. To a large extent, this is due to the idealized ozone distribution used in the current version of the model.

The bias in the meridional temperature gradient is reflected on the distribution of zonal-mean wind, particularly in the subtropical regions. As shown by the cross section in Fig. 8, the

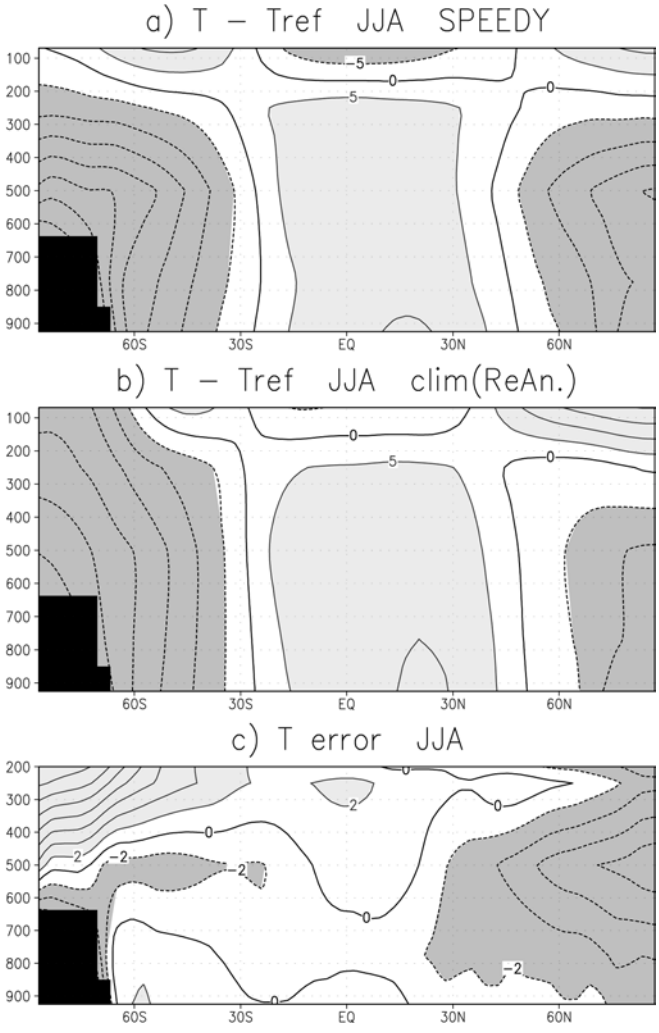

Fig. 7a–c As in Fig. 1, but for zonal-mean temperature in JJA

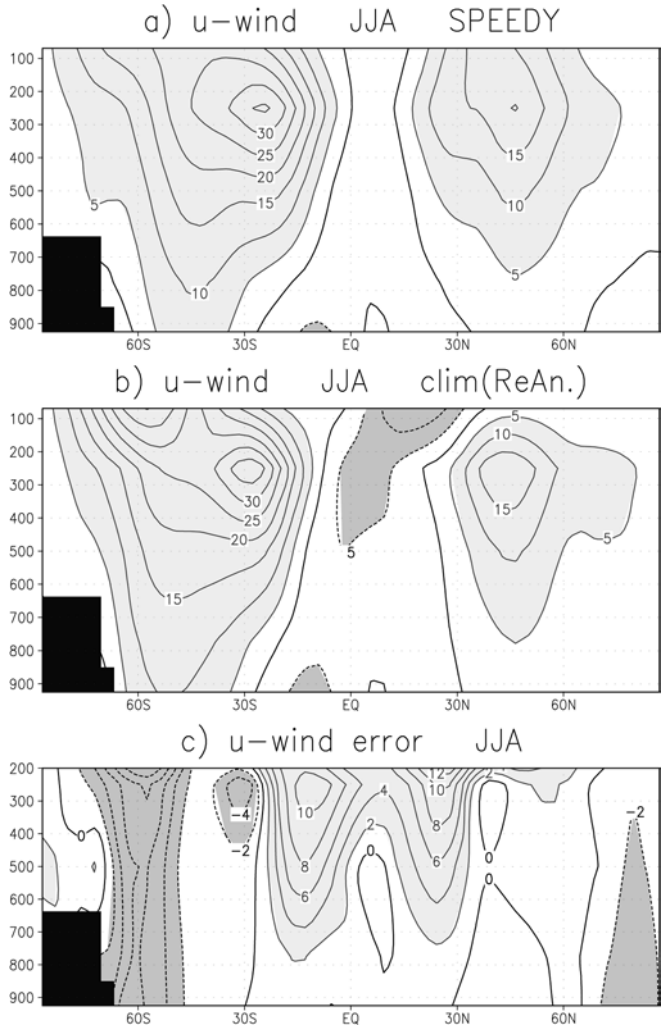

Fig. 8a–c As in Fig. 2, but for zonal-mean wind in JJA

upper-tropospheric westerlies extend too far into the tropics, leaving only a narrow region of zonal-mean easterlies at 250 hPa. At this level, the westerly bias reaches 10 m/s around 25 °N and 15°S, decreasing almost linearly with increasing pressure. A weak westerly bias covers most of the northern extratropics, leading to a midlatitude flow which is too spring-like in its zonally asymmetric component (not shown). In the southern extratropics, a northward shift of the jet causes a noticeable easterly error around 60°S.

As for the winter case, maps of 925-hPa zonal wind (not shown) indicate a good qualitative agreement in the location of westerly/easterly winds. However, the simulated near-surface zonal winds tend to be weaker than the observed in a number of regions, such as the whole Southern Ocean and large parts of the tropical oceans. In particular, with regard to the Asian monsoon circulation, the intensity of the low-level westerlies over the Arabian Sea, India and the Bay of Bengal is much underestimated, with a maximum located almost 10°S of the observed position.

The poor representation of the Asian monsoon is also evident from the mean rainfall distribution shown in Fig. 9. The rainfall maxima associated with the Tropical Convergence Zone (TCZ) in the Indian Ocean remain confined around 10°N, and the observed maximum over the Bay of Bengal is missing. On the other hand, the model produces large rainfall amounts on the southern slopes of the Himalayas. Over the west Pacific, rainfall is generally underestimated, while a better agreement with observations is found in the east Pacific and in the tropical Atlantic sector. The narrow latitudinal distribution of the JJA tropical rainfall in SPEEDY, compared to the observed climatologies, is highlighted in the zonal-mean profiles plotted in Fig. 9c.

3.4 Annual mean heat and water budgets

In view of the future use of SPEEDY as the atmospheric component of a coupled ocean–atmosphere system, it is appropriate to validate the simulated heat and freshwater budget at the surface, particularly over the oceans. These budgets are usually discussed on an annual mean basis; on this time scale, the assumption that total heat and water content of the atmosphere should not change is verified with very good approximation.

The annual-mean net heat flux into the ocean surface, computed as the algebraic sum of the net shortwave and longwave radiation, and the sensible and latent heat fluxes, is shown in Fig. 10a for the SPEEDY simulations and in Fig. 10b for the ECMWF re-analysis. The comparison shows a good correspondence in the location of all the main areas of heat sources and sinks. In particular, the oceanic heat sinks associated with the western-boundary currents in the Northern Hemisphere are evident, as well as the sources in regions of upwelling, along the equator and on the eastern margins of the tropical oceans. SPEEDY also successfully simulates the band of downward net flux along 50°S at the southern edge of the Atlantic and Indian oceans. On the other hand, the model tends to overestimate the amplitude of the heat sinks over

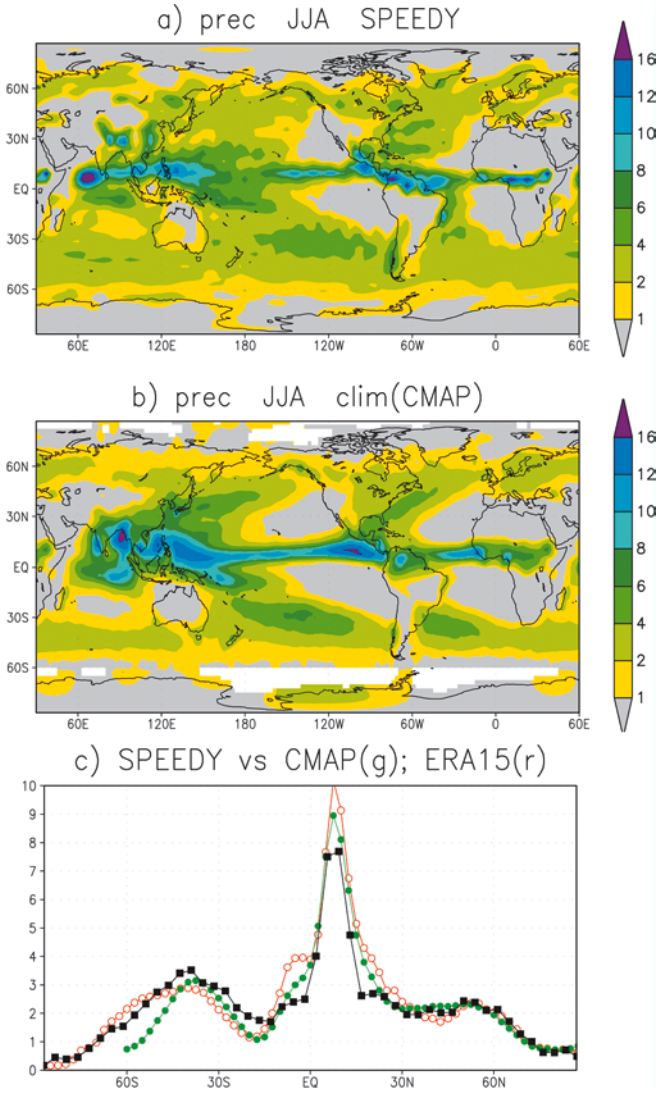

Fig. 9a–c As in Fig. 4, but for precipitation in JJA

the northern-midlatitude oceans. The ocean heat sources on the eastern edges of the tropical Pacific and Atlantic are also more intense than in the re-analysis, most likely because of the absence of a proper parametrization of stratocumulus clouds.

From the net heat budget at the surface and at the top-of-the-atmosphere, one can compute the net vertically integrated heat source for the atmosphere. For reasons of brevity, only the zonal-mean fields from SPEEDY and ERA are compared in Fig. 10c. (In order to interpret these zonal profiles in terms of divergence of the atmospheric meridional heat transport, the global-mean biases of the net heat budgets have been removed.) The meridional profile of the net atmospheric heat source shows a good agreement between model and re-analysis, with an equatorial local minimum of comparable depth, and a change from positive to negative values around 40°N and 40°S.

With regard to the mean meridional water transport, this can be inferred from the zonal mean distribution of precipitation minus evaporation (P–E), shown in Fig. 10d. With respect to ERA, SPEEDY underestimates P–E in the equatorial regions, and overestimates it in midlatitudes. A fairly good agreement is found in the subtropical areas, where P–E is negative. However, if the NCEP/NCAR re-analysis for the same years were used instead of ERA (not shown), a much closer agreement would be found over the whole tropical belt, while the differences over the northern extratropics would be larger. (Discrepancies between estimates of rainfall and surface fluxes between the NCEP/NCAR and ECMWF re-analyses are discussed by Kistler et al. 2001). In fact, from Figs. 4c and 9c, one can see that estimates of the amplitude of SPEEDY's errors for both tropical and extratropical rainfall depend significantly on the choice of the reference climatology.

4 Internal and forced variability in the boreal winter

4.1 Intraseasonal and interannual variability

In the previous sections, it has been shown that the current version of SPEEDY produces a much better simulation of the atmospheric mean flow in (boreal) winter than in summer. Because of this, and since the research projects in which the model is currently used are mainly focused on wintertime variability in the Northern Hemisphere, the documentation of model variability in this work will be limited to some basic statistics for the DJF season. A more detailed analysis of the modelled low-frequency variability and regimes, based on multivariate statistical analyses, will be presented elsewhere. Also, a documentation of the variability during the summer season will be postponed to a future model version, in which it is hoped that some of the current shortcomings in the mean flow will be alleviated.

In Fig. 11, the standard deviation of 500-hpa height over the northern extratropics is shown for three different time scales, comparing model results with NCEP/NCAR reanalysis. On the top row (Fig. 11a, d), high frequency variability is represented by the standard deviation of departures of instantaneous fields from 5-day means. In the middle row (Fig. 11b, e), intraseasonal low-frequency variability is assessed using deviations of 5-day means from running 60-day averages. Finally, in the bottom row (Fig. 11c, f), the interannual variability of DJF seasonal means are compared.

Looking first at high-frequency variability, the model provides a rather good simulation of the storm-track regions over the northern oceans. Over the Pacific, the simulated variability is lower than the observed one on the eastern side of the ocean, while a closer agreement is found at the entrance of the storm track. On the Atlantic, there is a more uniform underestimation of high-frequency variability (by about 20% of the observed standard deviation); however, a much larger discrepancy occurs over northern Europe, because of the incorrect intensity and orientation of the storm track. (This is not surprising, in view of the strong underestimation of the stationary wave amplitude over the European-Atlantic sector.)

In the distribution of intraseasonal low-frequency variability, the differences between simulations and analyses are more evident. Over both the Atlantic and the Pacific, the modelled low-frequency maxima are located southwest of the observed location. As for high-frequency variability, over the Pacific the reduction in magnitude mainly occurs on the eastern side of the ocean, while over the Atlantic the underestimation is more widespread and tends to increase with latitude.

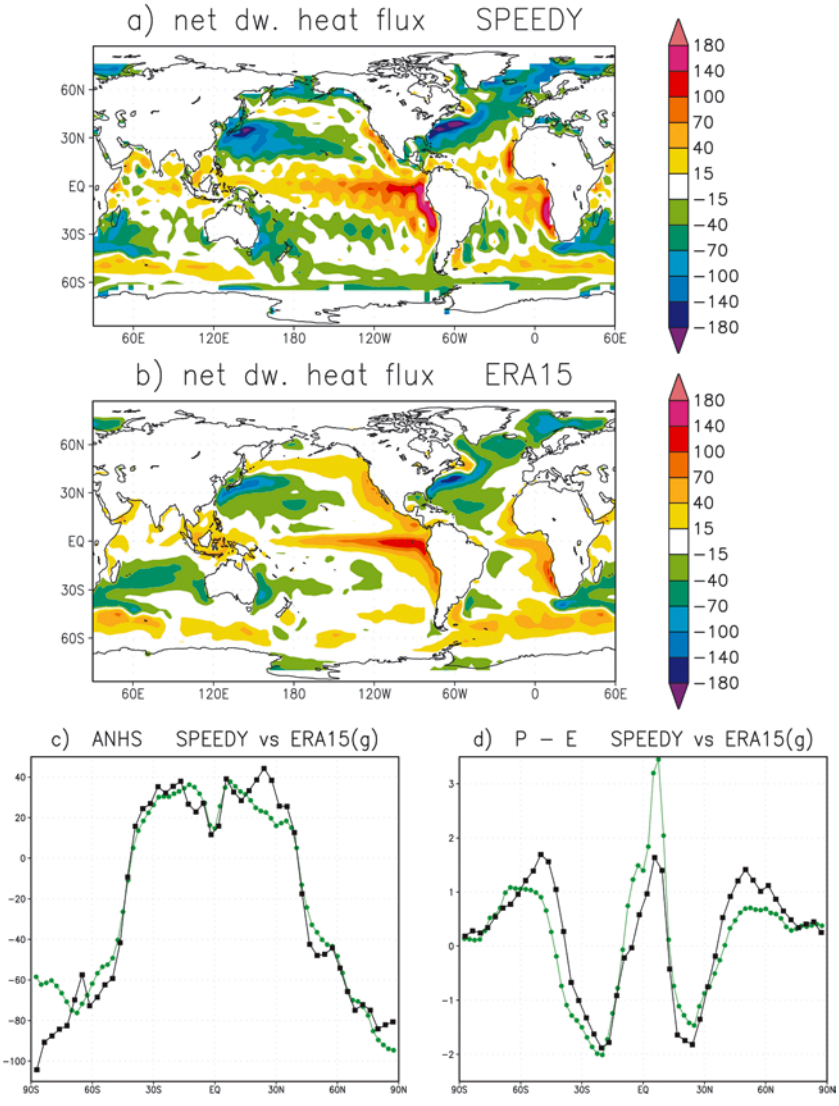

Fig. 10 Annual-mean heat and water budget. **a** net (downward) heat flux into the ocean surface, from the SPEEDY ensemble. **b** As in **a**, but from ERA. **c** Zonal-mean profiles of the net heat source into an atmospheric column, computed from the net heat fluxes at the upper and lower boundaries, for SPEEDY (*black*) and ERA (*green*). **d** Zonal-mean profiles of precipitation minus evaporation, for SPEEDY (*black*) and ERA (*green*)

Finally, considering the variability of seasonal means, one finds a rather good simulation of the position of the Atlantic maxima, while in the Pacific two separate maxima are located respectively to the west and to the east of the (single) observed maximum. Over both oceans, the modelled features show a 25% to 35% reduction in amplitude with respect to observations.

For both model and analysis data, the variability of seasonal means has been computed after removing the linear trend over the 1952–92 period, computed by a least-squares fit. Detrending the seasonal mean fields has little impact on the standard deviation maps shown in Fig. 11c, f, except for a reduction of the observed standard deviation in the North Atlantic. If one assumes that at least part of the observed trend is related to processes not represented in the model (e.g. changes in concentration of atmospheric ozone and greenhouse gases), a comparison between detrended data seems more appropriate. On the other hand, if part of the atmospheric trend arises as a response to the inter-decadal variability in SST, such a component should be reproduced in SST-forced integrations. This issue will be further discussed later.

It is well known that both the internal atmospheric dynamics and forcing from anomalous boundary conditions contribute to the interannual variability of seasonal means (see e.g. Straus and Shukla 2000). As shown, the amplitude of intraseasonal variability simulated by SPEEDY is lower than the observed amplitude, so it is highly likely that the contribution of internal dynamics to the modelled variability of seasonal means also has a smaller amplitude than in the real atmosphere. With regard to the simulation of the forced component, this may be validated by comparing modelled and analysed composite anomalies during ENSO (El Niño – Southern Oscillation) events.

For this purpose, the list of ENSO events given in the study by Hoerling et al. (1997) has been used (see their Table 1). Although the definition of a composite anomaly seems a straightforward task, because of significant interdecadal variations in the frequency of warm and cold events some care is needed to remove possible

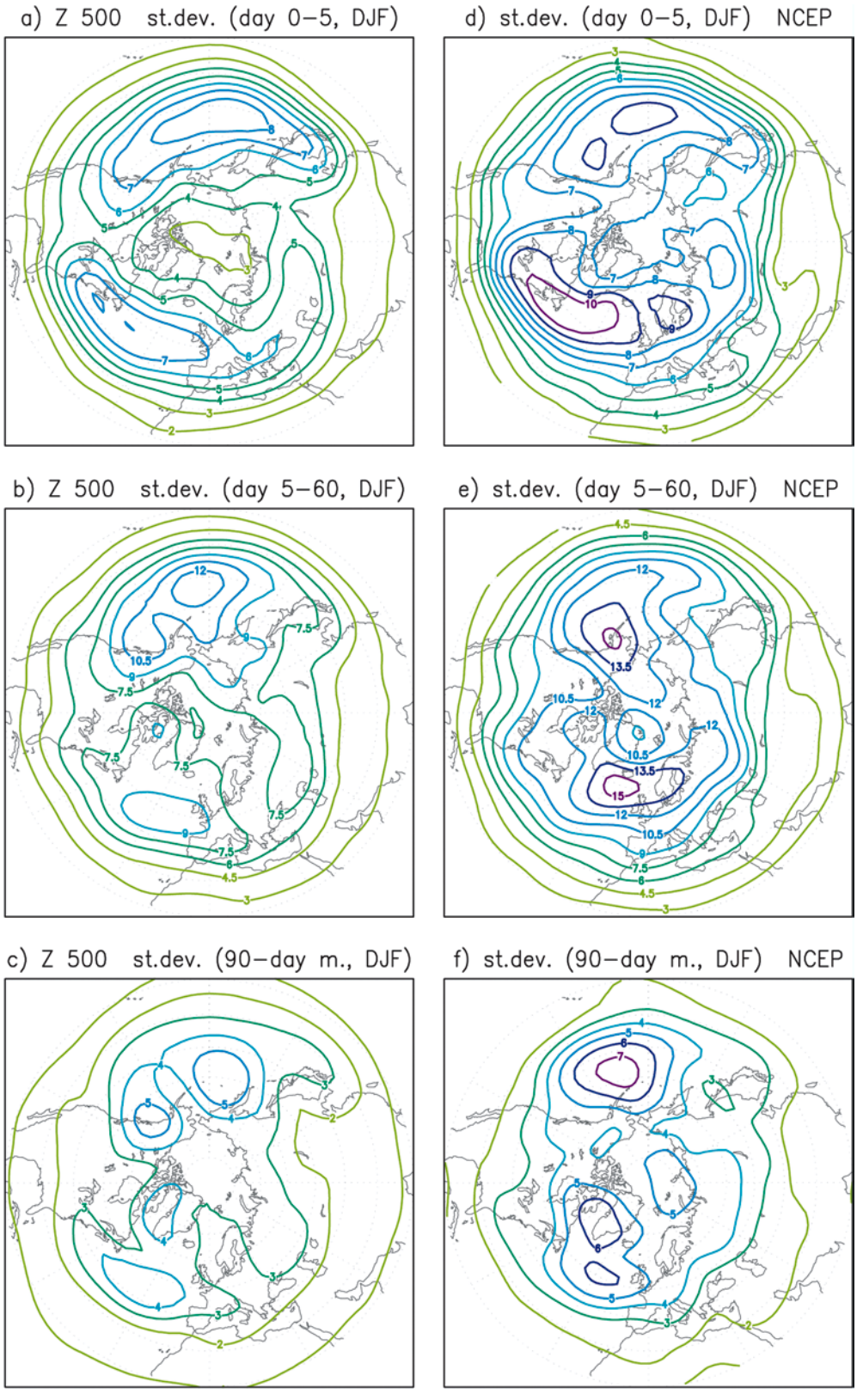

Fig. 11 Variability of 500-hPa height on different time scales in the DJF season, as shown by the standard deviation of: departures of instantaneous fields from five-day means (**a** and **d**, contour interval 1 dam); departures of 5-day means from running 60-day means (**b** and **e**, contour interval 1.5 dam); departures of 90-day means from the linear trend over the 1952–92 period (**c** and **f**, contour interval 1 dam). The statistics in **a**–**c** are from SPEEDY integrations, those in **d**–**f** from NCAR/NCEP reanalysis

'contaminations' by trends which may not be associated with ENSO. Focusing on warm (El Niño) events, a composite anomaly of 500 hpa height has been defined here as the difference between the average of the DJF means in the eight El Niño winters during the 1952–92 period, and the average of DJF means in all years either preceding or following the warm events (13 years in total, because of some overlap). Such a composite is

shown in the left column of Fig. 12 for the NCEP reanalysis (Fig. 12a) and the ensemble-mean of the SPEEDY integrations (Fig. 12b). In the right column, the composites from the three individual model integrations are plotted, to evaluate the reproducibility of such statistics.

Over the east Pacific, North America and parts of northern and central Asia, the simulated composite is

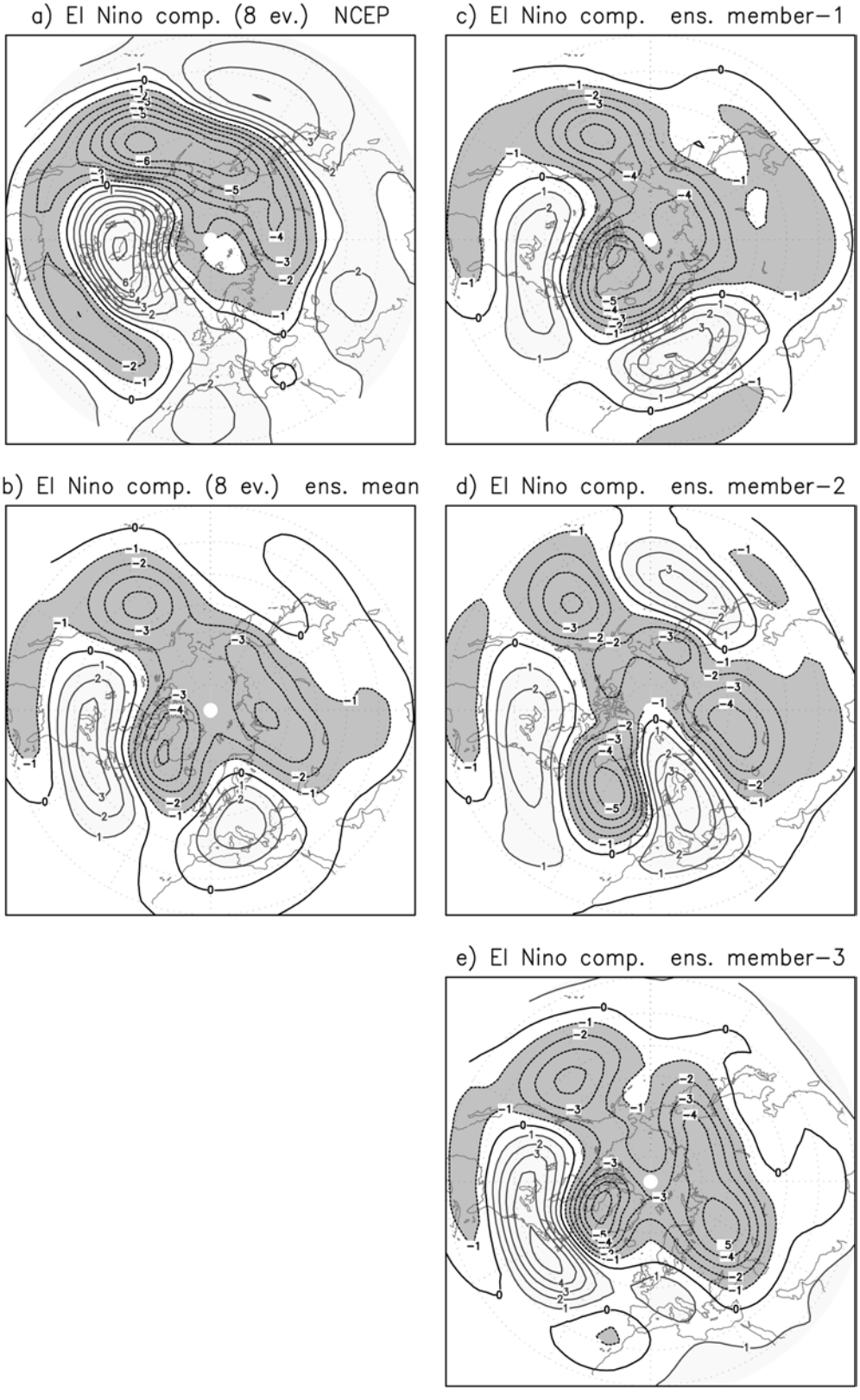

Fig. 12a–e Composite anomaly of 500-hPa height in DJF for 8 El Niño events during the 1952–92 period. **a** from NCAR/NCEP reanalysis; **b** from the ensemble mean of SPEEDY integrations; **c**–**e** from individual members of the SPEEDY ensemble. Contour interval 1 dam; negative contours *dashed*, *shading* as in Fig. 1

mostly in phase with the observed composite, with a quite correct location of the east Pacific negative centre. The amplitude of the response, however, is only between 50% and 70% of the observed signal in most areas. Over southwestern Europe, the sign of the model response is also correct, although the centre of the positive anomaly is somewhat shifted. The main discrepancy with respect to the analysis composite is the presence of a negative anomaly region centred over the southern tip of Greenland and covering a large part of the North Atlantic. The presence of this feature causes a weakening and the southward shift of the positive anomaly located over North America. Finally, the composite from individual experiments indicate a good degree of reproducibility for the composite response over the east Pacific, North America and Siberia, while (not surprisingly) fairly large differences between ensemble members can be found over the east Atlantic and Europe.

Although the reduced amplitude of the response might be partly due to problems with the model dynamics (which may also be responsible for the insufficient internal variability), errors in the simulation of the anomalous heat sources associated with SST anomalies are probably the most important cause of the weak midlatitude response. This is illustrated in Fig. 13, which compares the composite rainfall difference between three recent warm and cold ENSO events from the SPEEDY ensemble with the corresponding estimate from the CMAP dataset. In the tropical Pacific, the location of the regions of positive and negative differences agrees quite well with observations. On the eastern side of the ocean, the amplitude of the rainfall response is as large as (or even larger than) the observed signal, but in the central and western parts the simulated response is weaker. In particular, the positive maximum close to the dateline is twice as strong in observations than in the SPEEDY, and the decrease in rainfall over Indonesia and on the southern flank of the SPCZ are poorly reproduced. As far as the remote rainfall response is concerned, the SPEEDY simulations have the correct sign over the Caribbean region and southern Africa, while over South America and the tropical Atlantic the observed negative anomaly along the Equator is replaced by a dipolar structure where negative anomalies are shifted south of their observed location.

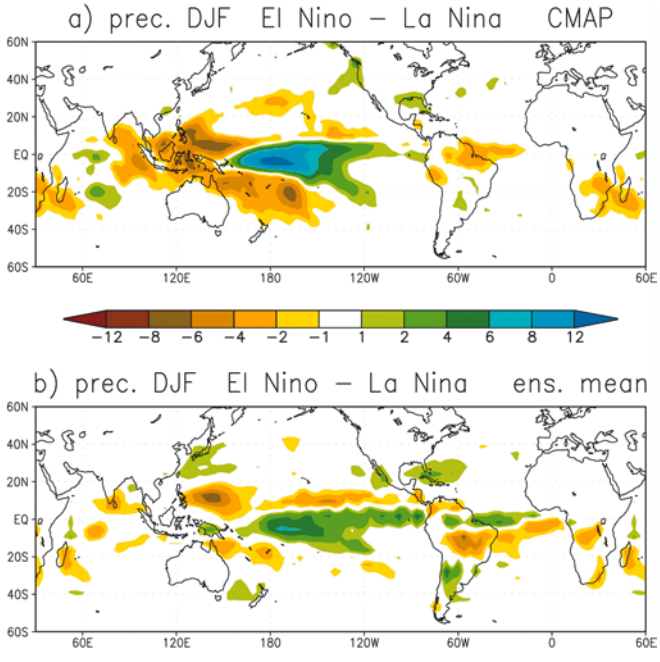

Fig. 13 Composite difference between precipitation in three El Niño and three La Niña events during DJF, in mm/day: **a** from CMAP data, **b** from the SPEEDY ensemble mean

4.2 Multi-decadal trends

For all time scales discussed so far, the modelled and observed variability have been compared on the assumption that the main dynamical and physical processes which generate the observed variability are reproduced in the model, albeit in a simplified way. If one considers the long-term trend of the northern extratropical circulation during the multi-decadal period covered by the SPEEDY runs, this assumption is no longer valid, since the impact of anthropogenic perturbations to the planetary radiative balance cannot be ruled out. However, the SST does show a trend in such a period (see Fig. 14a), which is related to an increased frequency of warm ENSO events, a widespread warming of the Southern Hemisphere oceans, a cooling of the midlatitude North Pacific and a predominance of the SST 'signature' of the positive phase of the North Atlantic Oscillation in the second half of the record (Zhang et al. 1997; Lau and Weng 1999; Cai and Whetton 2001).

In reality, some of these long-term SST changes (especially in midlatitudes) are likely to be the result, rather than the cause, of interdecadal atmospheric variations. Still, in the hypothesis that midlatitude SST anomalies exert a weak but positive feedback on the midlatitude atmospheric circulation (see Barsugli and Battisti 1998), interdecadal variations in SST should account for (at least) part of the interdecadal circulation changes in prescribed-SST simulations (e.g Rodwell et al. 1999).

Figure 15 compares the linear trend of 500-hPa height in the Northern Hemisphere, estimated from a least-squares linear fit to NCEP/NCAR reanalysis (Fig. 15a) and to SPEEDY ensemble means (Fig. 15b) in DJF. Although the simulated trend has a smaller amplitude than the observed one, this is not necessarily due to a model deficiency. Rather, one may notice a striking similarity between the two patterns in the Atlantic and Eurasian regions. It should be pointed out that, while the pattern of the reanalysis trend is in phase with the interannual El Niño response only over parts of the North Pacific and Asia, the similarity between the two patterns is much stronger for the SPEEDY simulations (see Fig. 12a, b). This result does not necessarily imply that the trend in SPEEDY is just a result of ENSO

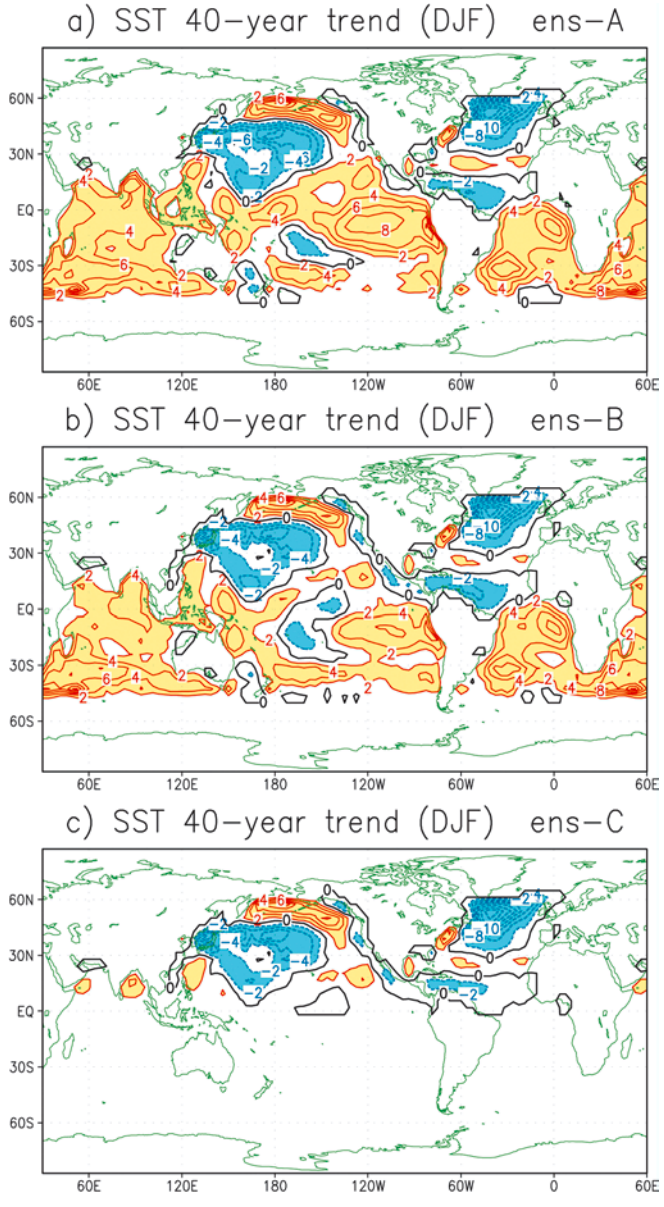

Fig. 14 Linear trend of SST in DJF, computed over the 40-year period from winter 1952/53 to winter 1991/92: **a** from original SST, used in the reference SPEEDY ensemble (ens-A); **b** from SST with ENSO signal removed, used in ensemble-B; **c** from SST with ENSO signal removed and anomalies confined to the Northern Hemisphere, used in ensemble-C. Unit and contour interval 0.1 K; negative contours *dashed*, *shading* as in Fig. 1

decadal variability. An alternative explanation is that a common, dominant mode of European-Atlantic variability may be affected by SST forcings located both in tropical areas (where the ENSO signal comes from) and in northern extratropical regions (where SST variations may arise from feedback mechanisms). In the real atmosphere, on the other hand, the ENSO signal over the Euro-Atlantic regions does not project strongly on the same mode (namely, the North Atlantic Oscillation) which displays the strongest interdecadal variability (see Pavan et al. 2000).

To test this hypothesis, two additional three-member ensembles have been run for the 1952–92 period, with modified SST. In one ensemble, the SST component correlated with the ENSO cycle was removed by computing, at every grid point, a linear regression against the "Niño3.4" index, and then subtracting the regressed signal from monthly mean anomalies. In a second ensemble, the ENSO-filtered SST anomalies (as defined already) were multiplied by a function of latitude, which progressively reduced the anomaly amplitude south of 15°N, and set all anomalies to zero south of the equator. The 40-year trends in these two modified SST datasets are shown in Fig. 14b, c respectively.

From the two ensembles with modified SST, the spatial patterns representing the linear trend of 500-hPa height were computed, as for the reference ensemble, and are shown in Fig. 15c, d respectively. For the ensemble using SST with only the ENSO signal removed, the 500-hPa height trend (Fig. 15c) shows a reduced amplitude in the Asian, Pacific and North American regions with respect to the ensemble with original SST (Fig. 15b). Over the North Atlantic, the signal has a comparable amplitude, but the location of the negative anomaly is no longer in phase with the observations (Fig. 15a). Therefore, the ENSO signal appears to contribute to the realism of the original simulation over the Atlantic sector. On the other hand, the results of the ensemble with SST anomalies confined to the northern extratropics suggest that the ENSO signal was not the dominant factor for the simulations of circulation trends over the Atlantic. In fact, the height trend from the latter ensemble (Fig. 15d) closely resembles the 500-hPa height anomaly associated with the NAO, and is clearly in phase with the observed trend in the European-Atlantic sector.

In conclusion, it appears that in SPEEDY simulations an interdecadal NAO-like signal may be excited both by tropical (ENSO-related) and extratropical SST anomalies, suggesting that contrasting results on the origin of NAO trends obtained from different state-of-the-art GCMs (e.g Rodwell et al. 1999; Hoerling et al. 2001) should not be considered as mutually contradictory.

5 Discussion and conclusions

In the previous sections, the formulation of an intermediate-complexity atmospheric GCM with simplified physical parametrizations (SPEEDY) has been presented, and its performance has been assessed comparing the simulated mean state and variability with the corresponding statistics from observational datasets. Taking into account the limitations imposed by the coarse vertical resolution and the simplified representation of physical processes, the model provides a rather realistic simulation of the atmospheric flow, especially during the boreal winter. Different ranges of atmospheric variability are reproduced in the SPEEDY simulations, from

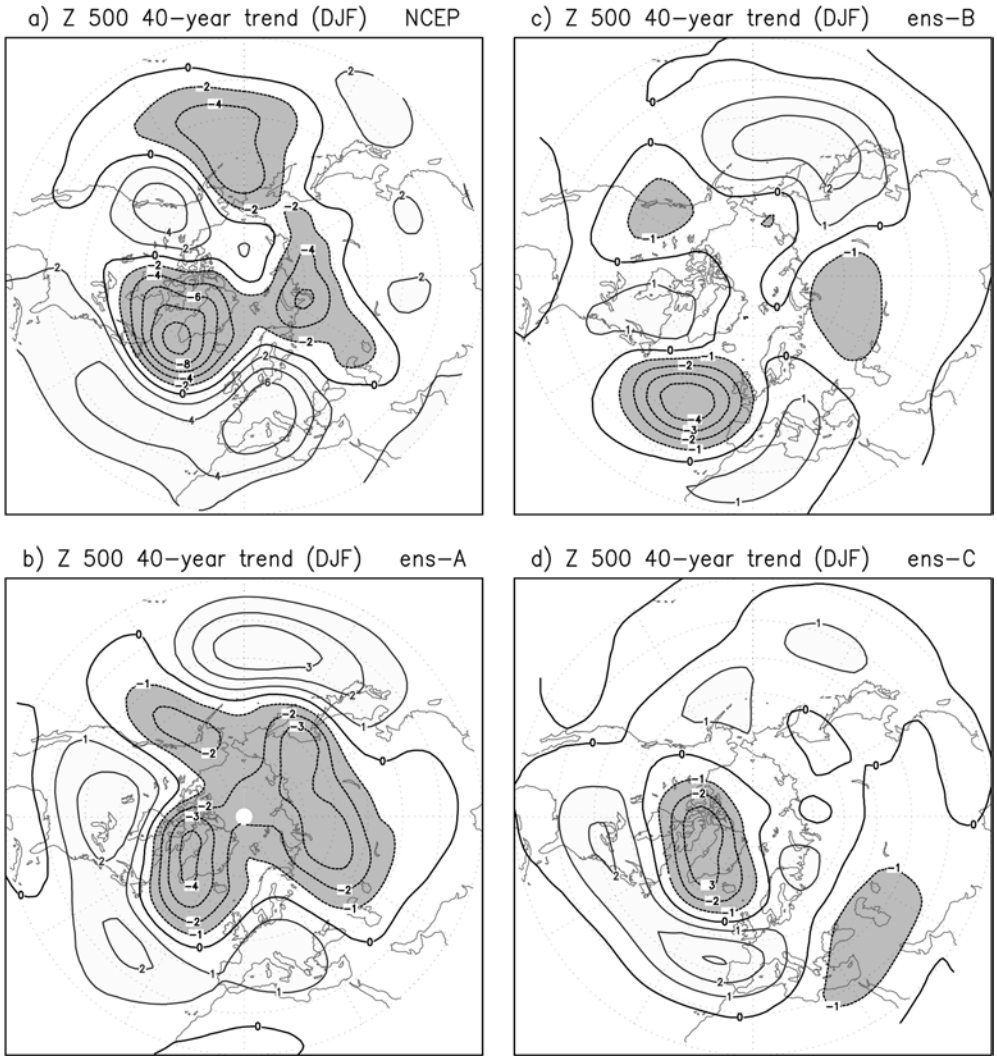

Fig. 15 Linear trend of 500-hPa height in DJF, computed over the 40-year period from winter 1952/53 to winter 1991/92: **a** from NCAR/NCEP reanalysis; **b** from the reference SPEEDY ensembles (ens-A); **c** from the SPEEDY ensemble using SST with ENSO signal removed (ens-B); **d** from the SPEEDY ensemble using SST with ENSO signal removed and anomalies confined to the Northern Hemisphere (ens-C). Contour interval 2 dam in **a**, 1 dam in **b**–**d**; negative contours *dashed*, *shading* as in Fig. 1

high-frequency fluctuations due to baroclinic systems to multi-decadal trends, although the amplitude of the modelled variability is usually smaller than its observed counterpart.

The reduced variability diagnosed in the SST-forced integrations presented here may be partly due to the fact that no variations in land surface parameters (apart from a prescribed seasonal cycle) were allowed in model version used for these experiment. Such a version should be considered as the atmospheric 'module' of a simplified climate model currently under development, in which interactive land-surface and ocean modules of different complexity will be coupled to the atmospheric component.

Naturally, legitimate questions may be asked about the usefulness of this modelling tool. Given the large systematic errors detected in the simulation of the summertime circulation, can one be sure that the reasonably good performance in winter does not arise from a balance of compensating errors, which however prevent meaningful conclusions about individual dynamical processes? Are there any advantages in using SPEEDY rather than a state-of-the-art GCM for long-term climate simulations?

With regard to the first question, one should bear in mind that a number of parameters, which in reality are complex functions of atmospheric variables, are represented as tunable constant coefficients in SPEEDY's simplified parametrization schemes. For some of these parameters, fixed values can be found which are representative of a wide range of atmospheric conditions. In other cases this is not possible, and unless more complex schemes are introduced, one has to choose values which will be more appropriate in certain regions and seasons than in others. When faced with such a situation, our choices have generally favoured an improved simulation of the climate statistics in boreal winter, since one of the main research task for which SPEEDY has been developed is the study of the statistical properties of the teleconnection patterns and flow regimes which characterize the Northern Hemisphere circulation during the cold season.

This specific research topic also provides an illustration of the range of dynamical problems in which the

computational efficiency of SPEEDY may be needed. In order to estimate the probability that interdecadal variations in the frequency of flow regimes (such as those documented by Corti et al. 1999) arose either from internal climate dynamics, or from some change in external forcing, one would need model integrations of (at least) several hundred years of length. Some simulations of similar length with state-of-art GCMs are currently available (e.g. Stouffer et al. 2000). However, if the role of different component of the climate system had to be tested using, for example, ocean and land-surface modules with different levels of complexity, a further increase in computer resources (up to one order of magnitude) would be required. Since the SPEEDY integrations described here have run at a computational speed of 25 min of single-CPU time per year of simulation on a SGI Origin 3800 computer, a 10-member ensemble of 400-year runs could be completed in one week using ten dedicated CPUs, even without any parallelization effort. It should also be mentioned that the 'lightness' of the SPEEDY code (only about 5000 lines of standard Fortran 77 code) makes it particularly suitable for numerical experimentation in academic and educational environments.

Finally, we wish to comment on the future use of the model and its possible developments. As mentioned, a more detailed analysis of low-frequency variability patterns and flow regimes in the northern extratropics, and of the interannual and interdecadal variability of their statistics, is currently under way. For this purpose, the coupling of SPEEDY to an oceanic mixed-layer model is being implemented.

Among future model developments, the implementation of an interactive scheme to represent anomalies in land-surface conditions is probably essential to achieve an improvement of monsoon circulations during the boreal summer. This should be accompanied by the use of a more appropriate closure scheme in the mass-flux convection. Simulations in all seasons may also be improved by a revision of longwave radiation scheme, which is currently producing significant biases in zonal-mean temperature at high latitudes. With regard to the current understimation of planetary wave amplitude and internal variability during winter, preliminary experiment with a 7-layer version of the model, in which a smoother change in layer thickness occurs at the upper and lower boundaries, suggest that part of these deficiencies may be alleviated by even a modest increase in vertical resolution.

As with any intermediate-complexity model, in the development of SPEEDY one has to reach a balance between the contrasting needs of the stronger 'intellectual control' which comes from the simplified formulation, and the desire to achieve an even closer similarity between simulations and reality. The optimal balance may vary according to the dynamical phenomenon to be investigated. Despite some notable shortcomings, it is felt that the balance reached with the current model version is good enough to address a range of dynamical problems, which represent some of the most debated issues in today's dynamical climatology.

Acknowledgements The author is grateful to M. Corbetta and R. Rizzi for the collaborative work on the development of the longwave radiation scheme, to L. Feudale and V. Pavan for their valuable diagnostic analyses, and to three anonymous referees for their useful and constructive suggestions. The numerical integrations were carried out at the CINECA Inter-University Computing Centre.

References

Barsugli JJ, Battisti D (1998) The basic effects of atmosphere–ocean thermal coupling on midlatitude variability. J Atmos Sci 55: 477–493

Bourke W (1974) A multilevel spectral model. I. Formulation and hemispheric integrations. Mon Weather Rev 102: 687–701

Brankovic C, Molteni F (1997) Sensitivity of the ECMWF model wintertime climate to model formulation. Clim Dyn 13: 75–101

Cai W, Whetton PH (2001) Modes of SST variability and the fluctuation of global mean temperature. Clim Dyn 17: 889–901

Corti S, Molteni F, Palmer TN (1999) Signature of recent climate change in frequencies of natural atmospheric circulation regimes. Nature 398: 799–803

Forster PM de F, Blackburn M, Glover R, Shine KP (2000) An examination of climate sensitivity for idealised climate change experiments in an intermediate general circulation model. Clim Dyn 16: 833–849

Gibson JK, Kallberg P, Uppala S, Hernandez A, Nomura A, Serrano E (1997) ECMWF re-analysis. Project report series. 1. ERA description. European Centre for Medium-Range Weather Forecasts, Reading (UK)

Held IM, Suarez MJ (1994) A proposal for the intercomparison of dynamical cores of atmospheric general circulation models. Bull Am Meteorol Soc 75: 1825–1830

Hoerling MP, Kumar A, Zhong M (1997) El Niño, La Niña, and the nonlinearity of their teleconnections. J Clim 10: 1769–1786

Hoerling MP, Hurrell JW, Xu T (2001) Tropical origins for recent North Atlantic climatic change. Science 292: 90–92

IPCC (2001) Climate change 2001: the scientific basis. In: Houghton JT, Ding Y, Griggs DJ, Noguer M, van der Linden PJ, Dai X, Maskell K, Johnson CA (eds) Cambridge University Press, Cambridge, UK, pp 881

Kalnay et al. (1996) The NCEP/NCAR 40-year Reanalysis Project. Bull Am Meteorol Soc 77: 437–471

Kistler et al. (2001) The NCEP-NCAR 50-year Reanalysis: monthly means CD-ROM and documentation. Bull Am Meteorol Soc 82: 247–267

Lau KM, Weng H (1999) Interannual, decadal–interdecadal, and global warming signals in sea surface temperatures during 1955–97. J Clim 12: 1257–1267

Opsteegh JD, Haarsma RJ, Selten FM, Kattenberg A (1998) ECBILT, a dynamic alternative to mixed boundary conditions in ocean models. Tellus 50A: 348–367

Pavan V, Molteni F, Brankoviç C (2000) Wintertime variability in the Euro-Atlantic region in observations and in ECMWF seasonal ensemble experiments. Q J R Meteorol Soc 126: 2143–2173

Randall DA (2000) General circulation model development: past, present and future. Academic Press, San Diego, pp 807

Robert AF (1966) The integration of a low-order spectral form of the primitive meteorological equations. J Meteorol Soc Japan 44: 237–245

Rodwell MJ, Rowell DP, Folland CK (1999) Oceanic forcing of the wintertime North Atlantic Oscillation and European climate. Nature 398: 320–323

Smith TM, Reynolds RW, Livezey RE, Stokes DC (1996) Reconstruction of historical sea surface temperatures using empirical orthogonal functions. J Clim 9: 1403–1420

Sperber KR, Palmer TN (1996) Interannual tropical rainfall variability in general circulation model simulations associated with the Atmospheric Model Intercomparison Project. J Clim 9: 2727–2750

Stouffer RJ, Hegerl G, Tett S (2000) A comparison of surface air temperature variability in three 1000-yr coupled ocean–atmosphere model integrations. J Clim 13: 513–537

Straus DM, Shukla J (2000) Distinguishing between SST-forced variability and internal variability in mid-latitudes: analysis of observations and GCM simulations. Q J R Meteorol Soc 126: 2323–2350

Xie P, Arkin PA (1997) Global precipitation: a 17-year monthly analysis based on gauge observations, satellite estimates and numerical model outputs. Bull Am Meteorol Soc 78: 2539–2558

Zhang Y, Wallace JM, Battisti DS (1997) ENSO-like interdecadal variability: 1900–93. J Clim 10: 1004–1020